International Journal of Scientific & Engineering Research, Volume 6, Issue 1, January-2015
ISSN 2229-5518

Anomaly in Elastic properties of cubic, tetragonal $BaFeO_3$ And Implications On $ab-initio$/DFT Computations of transition Metal Oxides

Ghous Narejo

Abstract

The *ab-initio* Hartree Fock, DFT-LDA, DFT-PWGGA, DFT-PBE and hybrid B3LYP potentials are employed to compute the optimized cubic and tetragonal phases of crystalline BaFeO3 by employing BILLY script and CRYSTAL09 code. ELASTCON and EOS algorithms are employed to compute the elastic constants and bulk moduli of the cubic phase. The equation of state bulk moduli of tetragonal phase are computed. The computational results on BaFeO3 phases are employed to generalize the findings. Due to highly correlated transition metal oxide physics the mechanical coupling in a variety of metal oxides is extracted by computing the FM/AFM exchange and total energy by UHF, SPIN-LDA, SPIN-PWGGA, SPIN-PBE and SPIN-B3LYP potentials. There is a novel evidence of the mechanical coupling in oxides.

Keywords: Elastic constant, Bulk modulus

1. Section I: Computations On Cubic and Tetragonal BaFeO3

Transition metal oxides have diverse applications in the field of data storage, sensing and actuation[91, 90, 81, 82, 99, 84, 85]. The recent advancements in the filed of fabrication of transition metal oxides have increased the possibilities of employing these materials for high density data storage, spintronic sensing and new logic design applications.

The success of new spintronic sensors has revived the interest in the crystalline structure and properties of the transition metal oxides[100]. The Fe transition metal is abundant in nature and its structure and properties have attracted the research interest throughout the history. However, there is a wide variety of the oxides of Fe transition metal. Oxides of Fe can occur in

perovskite form which has the highest magnetic moment [99] in perovskite crystalline structure. One of the perovskite oxides of Fe is $BaFeO_3$. The electronic structure and properties of this material are not explored very well.

There is scarcity of experimental data on the electronic structure and elastic properties of cubic and tetragonal phases of perovskite $BaFeO3$. It is suggested that this material is found in hexagonal [99], orthorhombic, cubic and tetragonal phases. There has been very few experimental studies limited to determining the crystalline geometery of the hexagonal and rhombohedral phases of $BaFeO_3$. No experimental study of bulk cubic and tetragonal phases of $BaFeO_3$ has been performed.

The experimental lattice of the pseudo-cubic and tetragonal crystalline structure for the epitaxial thin films are also observed from time to time [99, 84]. Therefore, the existance of pseudocubic and tetragonal structures in epitaxial thin films shows that the existence of high-pressure cubic and tetragonal phase can not be ruled out. However, the experimental evidence of the bulk cubic and tetragonal phases are not reported in the literature. Moreover, the absence of the experimental evidence for the cubic and tetragonal phases has led the computational scientists to predict [18] the computational values of bulk cubic and tetragonal phases with the experimental values for epitaxial thin films which is inappropriate. Successful usage of ferromagnetic and ferroelectric materials for various applications has motivated the research to explore the novel material phases.

Advancement of computational speed and processing power has led to a thrust in the computational effort[5, 6]. The novel phases of the novel class of perovskites are being discovered and experimented. CRYSTAL09 employes the first principles computational techniques to determine the electronic structure and properties of a wide variety of materials.

CRYSTAL09 code has unique crystalline geometry optimization algorithms which can be utilized for the innovative research into the novel phase discoveries. We employed BILLY script in CRYSTAL09 code to determine the crystalline structure of cubic BaFeO3. We employed all necessary checks to separate the numerical noise and physics.

The determination of crystalline structure led us to the task of determining the elastic properties of $BaFeO_3$. CRYSTAL2009 employs ELASTCON and EOS algorithms for the computation of elastic constants and bulk moduli of crystalline materials. There has been no experimental data on the electronic structure and elastic properties of $BaFeO3$. The major task was to ensure that the cubic and tetragonal phases are representative of physics and

not the numerical accident. Extreme care was taken in selecting the basis sets, geometry optimization algorithms and other techniques for computing the elastic properties.

1.1. Computational procedure

CRYSTAL09 code is employed to compute the optimized lattice parameters and elastic properties of cubic and tetragonal bafeo3 phases. The computational parameters were kept consistent throughout these computations. Shrinking factor was adjusted to 16 32, tolerances on SCF were kept as 999918. The tolerances on energy gradient were set to 9.

Computations were employed to optimize the crystalline structure of the high-pressure cubic and tetragonal phases of $BaFeO_3$. CRYSTAL09 has a unique combination of geometry optimization techniques to enable the computation of optimized crystalline structure. BILLY program is employed within CRYSTAL09 code to extract the optimized crystalline geometry.

The quality of geometry optimization results tested on the crystalline systems, for which the experimental data is known, have confirmed the validity of computational results.

The optimized lattice parameters, elastic constants and bulk moduli are computed by employing the ELASTCON and EOS algorithms for cubic $BaFeO_3$. The bulk moduli are computed with ELASTCON and EOS programs.

The computations of lattice parameters and elastic properties are performed on tetragonal $BaFeO_3$. The crystalline structure of tetragonal $BaFeO_3$ is computed and the optimized lattice parameters are obtained. The bulk moduli is computed by equation of state (EOS)[8, 7].

1.2. basis sets and potentials

During the computations of cubic and tetragonal crystalline phases of bafeo3, the basis sets and potentials are chosen from CRYSTAL09 basis set library [9, 16].

Two different basis set arrangements were chosen. The CRYSTAL09 [18] basis set library contains Fe-86-411d41G-towler-1992a and Fe-86-411d41G-towler-1992b for Fe atom and O-8-411-towler-1994 (modified muscat-1999), O-8-411-muscat-1999, O-8-411d11G-valenzano-2006, O-6-31d1-gatti-1994, O-6-31d1-corno-2006, O-8-411d1-bredow-2006 and O-8-411d1-cora-2005 for O atom.

The all-electon basis sets of Fe-86-411d41G-towler-1992a and Fe-86-411d41G-towler-1992b were employed for Fe while basis sets O-8-411d1-bredow-2006 and O-8-411d1-cora-2005 were utilized for O atom. The Ba-HAYWSC-311(1d)G-piskunov-2004 was employed for Ba atom.

The basis sets for Ba and O atoms are already tested during our computations on tetragonal $BaTiO_3$ and rutile TiO_2.

1.3. Billy script

Billy script [18] is employed within CRYSTAL09 code to compute the optimized crystalline structure of $BaFeO_3$. There are various options available within BILLY program.

The optimized crystalline structure is determined in BILLY program by employing the small variation in the lattice parameter value in the range of .0001 to 5 percent of a lattice parameter value provided as an external input.

The values of the energy for a range of lattice parameters are curve-fitted by a polynomial of third degree. The optimized lattice parameter is found at the lowest energy by the nonlinear least square curve-fitting of energy vs. lattice parameter values.

The accuracy of BILLY program was crosschecked by employing the nonlinear least square curve fitting using MATHEMATICA. The values of optimized lattice parameters computed with BILLY script and MATHEMATICA showed nice agreement in the optimized values of lattice parameters.

1.4. Computational parameters

The accuracy of the computations can be enhanced by selecting the tighter tolerances on the values of energy and its gradient as TOLINTEG 999918 and TOLDEE 9. The Pack Monkhorst shrinking factor was adjusted to 12 24 due to 3-d transition metal Fe. The SCF convergence was achieved by employing the BROYDEN technique as LEVSHIFT failed specifically during DFT computations. The numerical values of various parameters in BROYDEN were adjusted to as .00001, 50 and 5 during all computations.

1.5. ELASTCON and EOS algorithms

Computations of elastic constants and bulk moduli were performed employing ELASTCON and EOS programs. The main purpose of our computations was to confirm the validity of the computational results. To accomplish this we employed CRYSTAL and EOS codes to compare the bulk moduli results. In absence of the experimental results about the lattice parameters,

elastic constants and bulk moduli, the comparison of bulk moduli computed with relatively independent computational methods can confirm the validity of the computational results.

1.6. Crystalline Phases

Crystalline structures of transition metal oxides in perovskites are complex as well as promising to researchers. The high pressure phases of the perovskites can not be tested through experiments as it is very costly as well as complicated experimental exercise. Due to a high degree of progress in the computational science these materials can be tested through computational codes.

The CRYSTAL09 code can be employed to explore the novel high pressure phases of perovskites transition metal oxides. It is based upon the linear combination of atomic orbitals (LCAO) approach. The code is employed in combination with BILLY script to explore the crystalline geometry of the novel high pressure phases of $BaFeO_3$ transition metal oxide.

The cubic and tetragonal crystalline phases are discovered. These structures are not confirmed through experimental means. A careful study is done by optimizing the tolerances to improve the reliability of SCF convergence.

In absence of the experimental evidence of high pressure phases of $BaFeO_3$, we have employed the computations on perovskite oxides of other 3-d transition metals. In addition, we have utilized the experimental data on the crystalline structure and properties of $BaTiO_3$.

1.7. Computational results

The computational results for cubic and tetragonal phase are given for $BaFeO_3$.

1.8. Cubic $BaFeO_3$

The computational results for cubic phase are given for $BaFeO_3$.

1.9. Tetragonal $BaFeO_3$

The computational results for tetragonal phase of $BaFeO_3$.are given as well.

Table 1: **Computational values of lattice parameter in Angstroms, volume in $Angstrom^3$, density in $gram/cm^3$ and energy in a.u. for the cubic $BaFeO_3$ computed with HF, LDA, PWGGA, PBE and B3LYP potentials. See sections 1.1, ??, ?? and ?? for details about SCF parameters, computational analyses and conclusions about the effects of highly localized d-orbitals.**

	$a(A)$	$V_o(\mathring{A}^3)$	$Density(g/cm^3)$	$E(a.u.)$
HF	3.956	61.91	6.486	-1511.67809
LDA	3.819	55.73	7.204	-1510.95477
PWGGA	3.916	60.07	6.684	-1515.00777
PBE	3.9211	60.29	6.660	-1514.483489
B3LYP	3.921	60.29	6.656	-1514.619036
Exp. []	4.120			

Table 2: **The values of elastic constants and bulk moduli for cubic $BaFeO3$. These computations were done by using Hartree-Fock, DFT-LDA, DFT-PWGGA, DFT-BLYP, DFT-B3LYP and DFT-B3PW potentials. See sections 1.1, ??, ?? and ?? for details about SCF parameters, computational analyses and conclusions about the effects of highly localized d-orbitals. All values are in GPa.**

	C_{11}	C_{12}	C_{44}	B
LDA	194.28	225.78	131.71	215.28
PWGGA	107.77	155.23	88.37	139.41
PBE	108.05	150.96	89.50	136.65

Table 3: **baf-cub3Computational values of bulk moduli in GPa, volume in $Angstrom^3$, and energy in a.u. for the cubic $BaFeO_3$ computed with HF, LDA, PWGGA, PBE and B3LYP potentials. See sections 1.1, ??, ?? and ?? for details about SCF parameters, computational analyses and conclusions about the effects of highly localized d-orbitals.**

	B_{EOS}(GPa)	$V_o(\mathring{A}^3)$	$E_0(a.u.)$	B_{EL}(GPa)
HF	129.70	61.94	-1511.6746041	-
LDA	212.85	55.73	-1510.954822	215.28
PWGGA	142.16	60.04	-1515.007794	139.41
PBE	149.87	60.27	-1514.483511	136.65
B3LYP	146.31	60.35	-1514.6i90517	142.65

Table 4: **Computational values of lattice parameter in Angstroms, volume in $Angstrom^3$, density in $gram/cm^3$ and energy in a.u. for the cubic $BaFeO_3$ computed with HF, LDA, PWGGA, PBE and B3LYP potentials. See sections 1.1, ??, ?? and ?? for details about SCF parameters, computational analyses and conclusions about the effects of highly localized d-orbitals.**

	$a(A)$	$V_o(\mathring{A}^3)$	$Density(g/cm^3)$	$E(a.u.)$
HF	3.955	62.10	6.490	-1511.670839
LDA	3.831	56.24	7.14	-1510.948553
PWGGA	3.911	59.82	6.712	-1515.006266
PBE	3.916	60.09	6.682	-1514.481171904
B3LYP	3.917	60.13	6.677	-1514.616494

Table 5: **The values of elastic constants and bulk moduli for cubic $BaFeO3$. These computations were done by using Hartree-Fock, DFT-LDA, DFT-PWGGA, DFT-BLYP, DFT-B3LYP and DFT-B3PW potentials. All values are in GPa. See sections 1.1, ??, ?? and ?? for details about SCF parameters, computational analyses and conclusions about the effects of highly localized d-orbitals.**

	C_{11}	C_{12}	C_{44}	B
LDA	212.26	242.37	138.84	232.33
PWGGA	129.20	106.93	106.93	157.93
PBE	129.87	167.60	108.43	155.02

Table 6: **baf-cub6Computational values of bulk moduli in GPa, volume in $Angstrom^3$, and energy in a.u. for the cubic $BaFeO_3$ computed with HF, LDA, PWGGA, PBE and B3LYP potentials. Basis sets of Ba ECP, O 8411d11 and Fe 86411d11 were used. See sections 1.1, ??, ?? and ?? for details about SCF parameters, computational analyses and conclusions about the effects of highly localized d-orbitals.**

	B_{EOS}(GPa)	$V_o(\mathring{A}^3)$	$E_0(a.u.)$	B_{EL}(GPa)
HF	-	-	-	-
LDA	160.64	59.83	-1515.0062726	
PWGGA	155.87	60.07	-1514.4811825	-
PBE	155.87	60.07	-1514.4811825	-
B3LYP	157.94	60.18	-1514.6165046	-

Table 7: **baf-tet1Computational values of lattice parameters in Angstroms, volume in $Angstrom^3$, density in $gram/cm^3$ and energy in a.u. for the tetragonal $BaFeO_3$ computed with HF, LDA, PWGGA, PBE and B3LYP potentials. Basis sets of Ba ECP, O 8411d11 and Fe 86411d11 were used. See sections 1.1, ??, ?? and ?? for details about SCF parameters, computational analyses and conclusions about the effects of highly localized d-orbitals.**

	$a(A^0)$	$c(A^0)$	c/a	$V_o(\mathring{A}^3)$	$Density(g/cm^3)$	$E_o(a.u.)$
HF	3.797	4.099	1.079	59.13	6.791	-1511.872043
LDA	3.708	4.222	1.138	58.08	6.916	-1510.962842
PWGGA	3.860	3.860	1.00	60.24	6.67	-1515.012308
PBE	3.830	4.125	1.077	60.538	6.63	-1514.48623
B3LYP	3.881	4.043	1.041	60.90	6.59	-1514.62652

Table 8: **baf-tet2Computational values of bulk moduli in GPa, volume in $Angstrom^3$, and energy in a.u. for the cubic $BaFeO_3$ computed with HF, LDA, PWGGA, PBE and B3LYP potentials. Basis sets of Ba ECP, O 8411d11 and Fe 86411d11 were used. See sections 1.1, ??, ?? and ?? for details about SCF parameters, computational analyses and conclusions about the effects of highly localized d-orbitals.**

	B_{EOS}(GPa)	$V_o(\mathring{A}^3)$	$E_0(a.u.)$
HF	200.00	59.20	-1511.8782039
LDA	138.07	58.08	-1510.962836
PWGGA	130.95	59.79	-1515.0123155
PBE	127.62	60.53	-1514.4862532
B3LYP	221.70	62.37	-1514.6283632

Table 9: **baf-tet3Computational values of lattice parameters in Angstroms, volume in $Angstrom^3$, density in $gram/cm^3$ and energy in a.u. for the tetragonal $BaFeO_3$ computed with HF, LDA, PWGGA, PBE and B3LYP potentials. Basis sets of Ba ECP, O 8411d11 and Fe 86411d11 were used. See sections 1.1, ??, ?? and ?? for details about SCF parameters, computational analyses and conclusions about the effects of highly localized d-orbitals.**

	$a(A^0)$	$c(A^0)$	c/a	$V_o(\mathring{A}^3)$	$Density(g/cm^3)$	$E_o(a.u.)$
HF	3.799	4.099	-	59.19	6.784	-1511.8693632
LDA	3.773	3.954	-	56.29	7.133	-1510.949963
PWGGA	3.799	4.099	-	59.24	6.784	-1511.869364
PBE	3.867	4.050	-	60.57	6.629	-1514.4709459

Table 10: **baf-tet4Computational values of bulk moduli in GPa, volume in $Angstrom^3$, and energy in a.u. for the cubic $BaFeO_3$ computed with HF, LDA, PWGGA, PBE and B3LYP potentials. Basis sets of Ba ECP, O 8411d11 and Fe 86411d11 were used. See sections 1.1, ??, ?? and ?? for details about SCF parameters, computational analyses and conclusions about the effects of highly localized d-orbitals.**

	B_{EOS}(GPa)	$V_o(\mathring{A}^3)$	$E_0(a.u.)$
HF	197.55	59.24	-1511.869363
LDA	217.17	56.32	-1510.949958
PWGGA	197.55	59.24	-1511.869363
PBE	135.13	60.58	-1514.470945
B3LYP	-	-	-

2. Section II: Computations on Gnereric Transition Metal Oxides

The success of giant magnetoresistance (GMR) effect based devices has revived the interest in chargeless spin strain coupling in single and multiple phase of ferroics. [102, 81] Sirinivasan [81, 82] has explored the theoretical and experimental aspects of coupling in the thin films of ferroelectric and ferromagnetic composites. Tsymbal [99, 84, 85] has also carried out the first principles computations and fabrication of the interfaces between Fe and $BaTiO_3$. Sirinivasan and Tsymbal have discovered that the coupling between multiple phases is enhanced due to the elastic strain, atomic orbitals, chemical bonds at the boundary between the ferroelectric and ferromagnetic phases.

It has also been reported [53] in $La_xCa_{1-x}MnO_3$ that more than one phase can coexist in manganites due to compression of the lattice structure. Compression or expansion of the octahedral cage due to the change in the cation versus anion radius determines the phase transition from one phase to the other in manganites [52].

The studies of transition metals and their oxides by Goodenough [52], Maekawa [54, 49] and C. N. Rao [60, 55] is mainly focused on highly correlated transition metal orbitals. Tokura[51, 50] has also emphasized the interaction between the electron orbitals, crystalline lattice and pressure in the phase change of transition metal oxides. That work represents a detailed theoretical and experimental study of orbital electronics.

It is important to note that Sirinivasan and Tsymbal have performed the seminal research on the role of elastic strains, atomic orbitals and chemical bond in the field of phase coupling in ferroics. However, the detailed understanding of the interdependence between the elastic strain, atomic orbital, chemical bond and spin exchange has not been explored due to its complexity.

Numerous attempts have been made by Sirinivasan, Tsymbal and other researchers to model and fabricate thin film composites to couple the ferroelectric and ferromagnetic phases. The experiments on the elastic coupling of these thin film composites of separate phases have resulted in the weak coupling.

To the best of our knowledge, there has been no attempt to study the coupling between the ferromagnetic spin exchange and bulk strain in cubic perovskites. There is also a lack of systematized scientific theory and methods to understand the real causes of the weak coupling across ferroics.

The coupling between the electron spin and bulk strain is explored in

the cubic crystalline structures of a wide variety of transition metal oxides. First principles computational techniques are employed to compute the spin exchange coupling with the compression or expansion of the periodic crystalline lattice structure. The unrestricted Hartree Fock method is employed for the computation of ferromagnetic and antiferromagnetic spin exchange. The coupling between the ferromagnetic, antiferromagnetic spin exchange and lattice strains is computed for a wide range of 3-d transition metal oxide perovskites.

Studies of the lattice constant, spin resolved density of states, band gap and other electronic properties have been performed by first principles computational techniques [60]. We have employed the first principles computational techniques to the exchange energy for the ferromagnetic and antiferromagnetic spin exchange in the bulk $BaScO_3$, $BaTiO_3$, $BaVO_3$, $BaCrO_3$, $BaMnO_3$ and $BaFeO_3$.

These materials are chosen carefully to a wide range of transition metals for understanding the role of elastic strains on the exchange energy. Figures 3 and 4 show the periodic crystalline lattice of perovskite cubic $BaTiO_3$ and $BaFeO_3$. The supercell is utilized to compute the change in ferromagnetic and antiferromagnetic exchange energy. The compressive and tensile strains are introduced by decreasing or increasing the experimental lattice constant for each transition metal oxide in steps of .005 Angstrom.

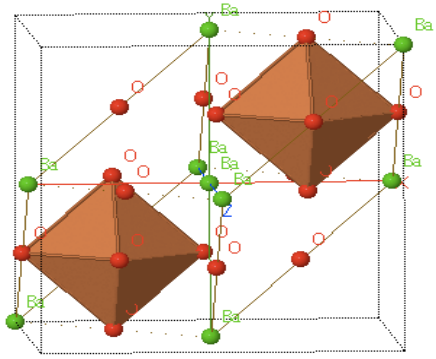

Figure 1: An octahedral is formed by O atoms having Fe atom in the middle. Green and red color spheres represent Ba, O and Fe atoms could not be seen as these are positioned in the middle of each cage in a perovskite $BaFeO_3$.

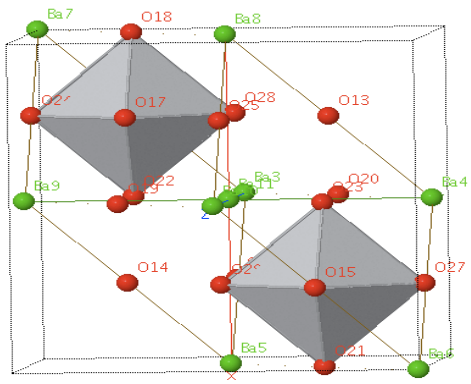

Figure 2: An octahedral is formed by O atoms having Fe atom in the middle. Green and red color spheres represent Ba and O while grey colored Ti atoms are positioned in the middle of each cage in a perovskite $BaTiO_3$.

3. Computational methods

The experimental values of lattice constants are used for the cubic crystalline geometry for each of the oxides. Basis sets for Ba and O atoms are kept consistent during all these computations as the basis set for the particular transition metal is changed. The Crystal09 code [61] is employed to compute the exchange energy for the ferromagnetic versus antiferromagnetic phase in each of the transition metal oxides. The unrestricted Hartree Fock (UHF) potential is employed during these computations. Care is taken to keep the Self Consistent Field (SCF) parameters consistent. However, the SCF parameters for $BaScO_3$, $BaVO_3$, $BaCrO_3$ and $BaMnO_3$ do differ from other material systems due to convergence problems.

The exchange energy is determined for the ferromagnetic as well as the antiferromagnetic phases for all the cubic crystalline systems as reported in Tables **??** - **??** and shown in Figures 3 - 10. After SCF convergence using the experimental lattice constant for each crystalline system, four additional computations are carried out on each crystal. The compression or expansion of the crystalline structure is done by introducing slight changes in the lattice constants.

Increments of .005 Angstrom value are introduced in the experimental lattice constant and the exchange energy is computed for the compression as well as expansion. Five separate computations are done for each of the crystalline systems. The computational strategy is repeated for a large variety

of crystalline systems for the oxides of third row transition metals to ensure the consistency of these computational results.

3.1. Quantum mechanical model

An extensive study has been done by Maekawa [49] on the wide variety of transition metal oxides known as manganites. The crystalline geometry and properties of cubic $BaMnO_3$ may be well - suited to the quantum mechanical model as discussed in refs. [51, 50]. This model is based upon the concept of a delicate balance between the crystal field and Hund's pairing energy. It is mainly framed upon the concept that the degeneracy in electron energies in transition metal oxides is partially lifted by the crystal field. The crystal field is formed among the electrons of the transition metal and oxygen atoms.

The model expresses the competition between the crystal field and Hund's pairing energy for the relaxed as well as strained crystalline structure. The phenomenon of ferromagnetic spin exchange, depending upon the highly correlated electrons in a crystal field, is also accommodated in the model. The ferromagnetic or antiferromagnetic spin exchange and its dependence upon the crystal field of the strained lattice is also discussed. This model can be applied to manganites (AMO_3), titanates ($ATiO_3$) and vanadates (AVO_3) as the crystal field splitting is predominant and is relevant in all the material systems discussed as in ref. [49]. The generic Hamiltonian for a transition metal oxide is

$$H_{eff} = H_{hund} + H_{t_{2g}} + H_{e_g} \tag{1}$$

The H_{e_g} term in Eq. 1 expresses the energy component due to e_g valence electrons of the transition metals σ- bonded with the p- valence electrons of O atoms in an octahedral complex. Whereas, the $H_{t_{2g}}$ term expresses the energy component due to t_{2g} electron which are π- bonded the p- electrons of O atoms.

The term H_{hund} expresses the Hund energy component for the electrons as

$$H_{hund} = J_H \sum_i S_i S_i^{t2g} \tag{2}$$

The second energy component in Eq. 1, due to the electrons localized to a t_{2g} transition metal orbital, contributes to antiferromagnetic spin exchange.

$$H_{t_{2g}} = J_{ij} S_i^{t2g} S_j^{t2g} \tag{3}$$

Equation 4 expresses the components of H_{e_g} term

$$H_{e_g} = \triangle \sum_i L_{iz} + \sum_{<ij>\sigma\gamma\gamma'} t_{\gamma}^{ij\gamma'}(a_{i\gamma\sigma}^{\dagger} a_{j\gamma'\sigma}) + \sum_{\beta} H_{U_\beta} \tag{4}$$

In Eq. 4, the subscripts i and j express the nearest neighbors on ionic sites, and $a_{i\gamma\sigma}^{\dagger}$ and $a_{j\gamma'\sigma}$ are the creation and annihilation operators, respectively. Small changes in the electron energy are introduced due to the compression and expansion of the lattice constant as shown in Table **??**-**??** and Figures 5 to 10.

The term t in Eq. 4 expresses the kinetic energy of e_g electrons in $BaMnO_3$, $BaCrO_3$ and $BaFeO_3$ which competes with electrostatic energy term U for lowering of energy. Eq. 4 takes into account the kinetic energy of electrons delocalized due to strains on the σ - bonded e_g and p valence electrons. The electrons hopping between the cation and anion sites are termed as i and j.

$$t = \sum_{<ij>\sigma\gamma\gamma'} t_{\gamma}^{ij\gamma'}(a_{i\gamma\sigma}^{\dagger} a_{j\gamma'\sigma}) \tag{5}$$

$$t_{ij}^{\gamma\gamma'} = \alpha_{\gamma\gamma'} t_{oij} \tag{6}$$

The electrostatic energy term U expresses the on-site electron correlation in transition metal cations resulting in the electron localization on transition metal sites. The symbol t in Eq. 5 is the hopping integral for electrons transferred under the action of strains from ions termed as i and ions at the nearest neighbor sites termed as j. The term J_H shows the dependence of ferromagnetic exchange energy on the Hund's pairing energy and electronic correlation U. Hund's energy has energy components due to the spins of t_{2g} and e_g electrons which are well - localized on each transition metal site due to electron correlations as shown in Eq. 7.

$$J_H = H_U + H_{U_{t_{2g}}} + H_{U_{e_g}} \tag{7}$$

The term $\triangle\epsilon$ in Eq. 8 signify the change in the crystal field energy due to strain. The term $\sum_i T_i$ expresses the change in the spin angular momentum of orbitals due to the effect of strain.

$$\triangle\epsilon = \triangle \sum_i T_i \tag{8}$$

4. Results and discussion

A cluster of atoms each consisting of 02 unit cells was used during computations of of total energy with Hartree Fock, DFT-LDA, DFT-PWGGA and DFT-B3LYP potentials for all crystalline systems with a being the optimized lattice parameter computed with billy script [61].

$$\begin{pmatrix} a/2 & a/2 & a \\ a/2 & a & a/2 \\ a & a/2 & a/2 \end{pmatrix}$$

The matrix of atoms was used to compute the ferromagnetic and antiferromagnetic properties and their dependence on variations in the lattice structure of each material system.

The unrestricted Hartree Fock method, implemented in the $Crystal09$ code, was employed to compute changes in exchange energy when small strains were employed on the unit cell of cubic crystalline ABX_3. The lattice sites A and X contained Ba and O atoms while B site was replaced with Sc, Ti, V, Cr, Mn and Fe.

The experimental values of lattice constants were used for the computations of exchange energy. Small increments were employed for the compression as well as expansion of lattice constant around the equilibrium for the cubic ABX_3.

The strains were introduced by changing the lattice constant. These strains were employed as small increments of .005 Angstrom on the experimental lattice constant of each material. All computational parameters were kept identical to ensure the consistency in computational results. For cubic $BaTiO_3$, $BaMnO_3$ and $BaFeO_3$, the application of bulk strains resulted in a change in the electron exchange, ferromagnetic exchange and antiferromagnetic exchange energy.

An interdependence between the electron exchange for ferromagnetic, antiferromagnetic exchange and lattice strain is found. There is an increase in the electron exchange for the expansion of lattice constant, whereas the decrease in lattice constant values results in a decrease of the exchange energy for the ferromagnetic and antiferromagnetic exchange.

It is observed that the exchange energy is lowered and enhanced consistently with the compression and expansion respectively for cubic crystalline systems of $BaScO_3$, $BaTiO_3$, $BaVO_3$, $BaCrO_3$, $BaMnO_3$ and $BaFeO_3$.

While computing the exchange energy for the ferromagnetic and antiferromagnetic exchange the Ti atom in B site in the ABX_3 was replaced with transition metals closer to Ti in the periodic table. The purpose of this arrangement was multifold with the main focus being the ferroic properties of $BaTiO_3$.

Confirmation about the consistency in computational results and detecting the dependence of exchange energy on various factors was necessary. The important factors such as lattice constant, ionic radii at sites A and B, electronic configuration of the d orbital, and the nature of chemical bonding needed particular attention.

The computational method was kept as identical as possible for all crystalline systems. It was found that the energy for antiferromagnetic exchange is smaller than the ferromagnetic exchange in $BaTiO_3$ thereby confirming it as an antiferromagnetic material. On the other hand, energy for the ferromagnetic exchange is lower in all other material systems. The ferromagnetic exchange for $BaScO_3$ needed special attention as it has fewer electrons than Ti.

The computational results for the lattice constant vs. exchange energy for ferromagnetic and antiferromagnetic exchange are shown in Table **??** - **??** and Figures 5-7. A degree of consistency in results and uniformity of trend can be clearly seen in Figures 5-7 except for Figure 9. The oscillatory trend for the $BaVO_3$, $BaCrO_3$ and $BaMnO_3$ material systems may be due to the interplay between the electron repulsions between transition metals and oxygen atoms leading to the effects on the electrostatic and hybridization nature of chemical bonding. In Tables **??** - **??** below the $E_{fm.}$, $E^{fm.}_{exch.}$, $E_{afm.}$ and $E^{afm.}_{exch.}$ represents the total energy computed with ferromagnetic spin exchange, ferromagnetic spin exchange energy, total energy with antiferromagnetic exchange and antiferromagnetic spin exchange energy.

In Table **??**, computational results of cubic $BaScO_3$ with Hartree Fock, DFT-PWGGA and DFT-B3LYP are shown as ferromagnetic. DFT-LDA computations revealed it as an antiferromagnetic material. As can be see in Table **??**, computational results of of open shell computations on cubic $BaTiO_3$ done with Hartree Fock, DFT-PWGGA confirmed it as antiferromagnetic material. DFT-B3LYP showed no difference in open shell computations for spins in same vs. opposite directions.

Whereas in Table **??**, open shell computational results of cubic $BaVO_3$, done with Hartree Fock and DFT-B3LYP, confirmed it a ferromagnetic mate-

rial. DFT-PWGGA showed it an antiferromagnetic material and DFT-LDA could not show any difference between energies for spins polarized in same vs. opposite directions.

On the other end as shown in Table **??**, open shell computational results of cubic $BaCrO_3$ done with Hartree Fock and DFT-PWGGA showed it an antiferromagnetic material respectively. DFT-PWGGA showed it a ferromagnetic material and DFT-B3LYP did not show any difference beyween energies for spins polarized in same vs. opposite directions.

Moving further to Table **??**, open shell computational results of cubic $BaMnO_3$, done with DFT-LDA, showed it a ferromagnetic material respectively. DFT-B3LYP did not showed it an antiferromagnetic material. Finally, the Table **??** shows the open shell computational results of cubic $BaFeO_3$ are done with Hartree Fock and DFT-B3LYP showing it a ferromagnetic material respectively. DFT-PWGGA and DFT-LDA did not show any difference beyween energies for spins polarized in same vs. opposite directions.

The spin overlap between nearest neighbors were computed with Mulliken population for Hartree Fock, DFT-LDA, DFT-PWGGA and DFT-B3LYP potentials. The Figure 7-9 shows the variations in Hartree Fock exchange energy due to spin density overlap in $BaVO_3$, $BaCrO_3$ and $BaMnO_3$. On the other hand, Figure 5, 6 and 10 shows no fluctuations in the exchange energy for $BaScO_3$, $BaTiO_3$ and $BaFeO_3$. The oscillatory vs. linear trend between the former and latter is due to the different impact of the crystalline lattice on the ferromagnetic properties of each sub-group of 3-D metals. Moreover, the former sub-group has an unstable or pseudo cubic phase which may have caused fluctuations in values of energy.

It can be seen in Tables **??**-**??** and Figures 5-10 that there is a lowering of ferromagnetic exchange energy due to compression of lattice. The lowering of the exchange energy is caused by the lifting of the degeneracy in electron energy due to the repulsion between the electrons occupying the oxygen p and transition metal d orbitals. The impact of the compression and expansion of the the lattice is observed on all the transition metal oxides selected. For $BaVO_3$, $BaCrO_3$, $BaMnO_3$ and $BaFeO_3$, which have more electrons in e_g energy levels, the degeneracy of these energy levels is partially removed due to the compression of lattice as these energy levels face the oxygen p orbitals forming a σ bond with the latter. As the number of electrons in d orbitals are decreased, the electrons at t_{2g} energy levels are less affected by the lattice strains. Electron delocalization effects due to strain are less prominent in $BaTiO_3$ specifically.

On the other hand, the expansion and compression of the lattice volume results in a decrease and increase in the ferromagnetic spin exchange energy which may point at the weakening and strengthening of the ferromagnetic properties of the material if the critical volume the particular material is not surpassed. As atoms are pulled apart, there is an increase in the electron exchange due to the reduction in overlap of atomic orbitals via the nearest neighbor atoms.

The primary effect of the external pressure on the transition metal oxides is to compress or expand their bond lengths connecting the transition metal and oxygen atoms in a perovskite. The expansion and contraction of the bond length results in the weakening or strengthening of the ferromagnetic exchange coupling of the transition metal e_g electrons via oxygen p electrons of the nearest - neighbor oxygen atoms.

Moreover, the exchange interaction is facilitated by the compression only if there are enough number of electrons in e_g sub-orbital. This can be observed in the computational results obtained for $BaCrO_3$, $BaMnO_3$ and $BaFeO_3$. Less variation in the exchange energy as a function of lattice strain strengthens the argument in favor of the localized nature of t_{2g} and e_g electrons. During compression, the Crystal Field Stabilizing Energy (CFSE) is lowered thereby supporting the lowering of exchange energy in comparison with the Hund's energy. This phenomenon of exchange energy lowering by the compressive strains may have strengthened the ferromagnetic properties as shown in computational results. However, this effect is weak in $BaTiO_3$. On the other hand, the effects of axial compression on perovskite are not discussed in this paper.

The oxides of transition metal have varied number of electrons in their highly correlated d orbitals. The electron exchange in transition metal sites via O atomic sites determines their ferromagnetic properties as shown in Tables **??**-**??**. The contracted wavefunctions of d electrons in $BaScO_3$, $BaTiO_3$, $BaVO_3$, $BaMnO_3$ and $BaFeO_3$ experience the varied degree of competitive forces [**?**] of the coulomb repulsion versus hybridization resulting in the ferromagnetic versus antiferromagnetic properties. The former try to localize the electrons at atomic lattice sites while the latter favors the overlaps with p and d orbitals of O and transition metal to delocalize these electrons. The forces of coulomb repulsion and hybridization are varied by lattice strain which results in the delocalization of electron spin density at each transition metal and O atomic site.

It has been observed that the primary factor that determines the nature

of electron exchange being antiferromagnetic versus ferromagnetic is the position of electrons in d orbitals of transition metal oxides. In addition to this, the case of $BaScO_3$ needs additional reasoning as the Sc atom has fewer electrons than Ti but has resulted in a ferromagnetic property. The case of $BaScO_3$ needs to be explored in depth to explore the physics behind the cation radius, nature of chemical bonding and the orbital overlap leading to its ferromagnetism.

Another factor that may affect the ferromagnetic or antiferromagentic exchange is the amount of strain on the lattice of each crystalline material. A trend can be seen in all computations as there is a consistent decrease in exchange energy for the compression and increase in exchange energy for expansion of lattice volume as shown in Tables confirming the influence of lattice strain on the electron exchange.

The chemical bond in transition metal oxides is a combination of covalent and ionic parts. The covalent and ionic parts vary as the transition metal ionic radius increases from Sc to Fe. The contribution of ionic bonding is increased as the number of electrons in transition metals are increased with more impact on the exchange energy from lattice strain.

The computational results of $BaScO_3$, $BaTiO_3$ and ferromagnetic $BaVO_3$, $BaCrO_3$, $BaFeO_3$ are due to the variation in nature of chemical bonding from strongly covalent to moderately ionic. The chemical bonding is controlled by the ionic radius of transition metal and its overlap with oxygen. A large change is seen in exchange energy as the ionic radius of transition metals is enhanced from Sc to Fe introducing the pressure on the octahedral cage formed between transition metal and oxygen atoms.

The weak nature of π bonding between Ti-O t_{2g}-p sub-orbitals respectively results in antiferromagnetic exchange in $BaTiO_3$ as shown in Table **??**. While σ bonding between transition metal e_g and oxygen p electrons in V to Fe results in ferromagnetic exchange as can be seen in Tables **??**-**??** .

If e_g orbital of any transition metal ion is occupied by an electron, it changes in the position of atoms and lattice parameters coupled with Jahn Teller and lattice strain distortions. The change in the position of atoms, usually coupled strongly with e_g electrons, may not happen in $BaTiO_3$ as there are no electrons to occupy e_g energy levels. However, any excitations of t_{2g} electrons, which are favorable in energy, brought by axial pressure may change the ferromagnetic properties. The weak effect of compressive strains on $BaTiO_3$ can be observed in Table **??** and Fig. 6.

The ferromagnetic spin exchange in case of $BaVO_3$, $BaCrO_3$, $BaMnO_3$

and $BaFeO_3$ is due to the double exchange between transition metal e_g and oxygen p electrons. The deficiency of the ionic character and less number of electrons in $BaTiO_3$ results in an antiferromagnetic spin exchange.

It is observed in Tables **??**-**??** that the compression results in the partial removal of degeneracy in electron energies. The degeneracy that was partially lifted by the crystal field splits the d orbital energies into e_g and t_{2g}. The e_g consist of $dx^2 - y^2$ and dz^2 levels which are split up further into distinct energy levels due to the compression.

The chemical bonding in transition metals has electrostatic and covalent character resulting in an overlap of electron wave functions. The transition metal e_g and oxygen p sub-orbitals form a stronger σ bond whereas the transition metal t_{2g} and oxygen p sub-orbitals form a weaker π bond. The σ and π has consequences to determine the competition for the lowering of energy for the ferromagnetic versus antiferromagnetic exchange. The ferrromagnetic properties of transition metal oxides are a result of ionic character of the bond formed between the transition metal and oxygen.

From the computed results shown in Table **??** - **??**, it is seen that in case of lattice volume expansion, the localized energies of highly correlated d orbitals are not sufficiently perturbed by the crystal field. The crystal field weakens as the position of atoms in a unit cell are pulled farther apart. Initially, there may be strengthening of the electrostatic character at the cost of weakening of the hybridization character of bonding. Later, there may be a weakening of the electrostatic bonding character, too.

5. Section III: Concluding Remarks

We have employed first principles computational techniques to compute the mechanical properties namely elastic constants and bulk moduli for cubic and tedtragonal phase $BaFeO_3$. The computational results show the interer-ence between the electron and the lattice resulting in the complexity leading to partial failures in some cases. These findings are later on employed to compute the coupling between the charge and the lattice. The total energy for the spin alignments in similar and opposite directions is computed for a wide variety of perovskite cubic crystalline transition metal oxides. It is observed that the compressive strain on the bulk lattice structure results in the lowering of the spin exchange energy due to the degeneracy lift off and overlap between the orbitals.

It is also seen that the coupling is weak in case of weak orbitals overlaps. During these computations, it is observed that the compressive strain lowers the exchange and total energy in all transition metal oxides. The lowering of the energy may be attributed to the stronger overlap between transition metal e_g and p orbitals forming a σ bond.

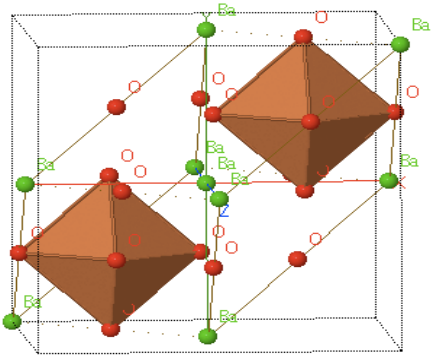

Figure 3: An octahedral is formed by O atoms having Fe atom in the middle. Green and red color spheres represent Ba, O and Fe atoms could not be seen as these are positioned in the middle of each cage in a perovskite $BaFeO_3$.

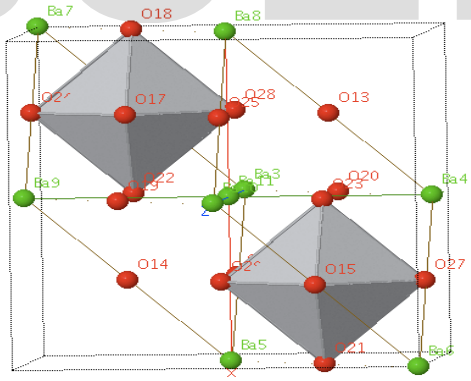

Figure 4: An octahedral is formed by O atoms having Fe atom in the middle. Green and red color spheres represent Ba and O while grey colored Ti atoms are positioned in the middle of each cage in a perovskite $BaTiO_3$.

6. Bibliography

[1]

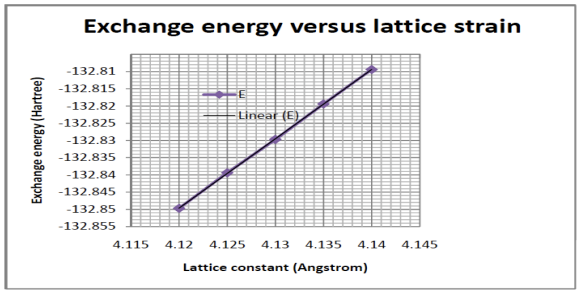

Figure 5: Exchange energy vs. lattice strain for cubic $BaScO_3$. A decrease in exchange energy can be seen for the compression of lattice. The straight line is drawn to signify the linearity of the trend.

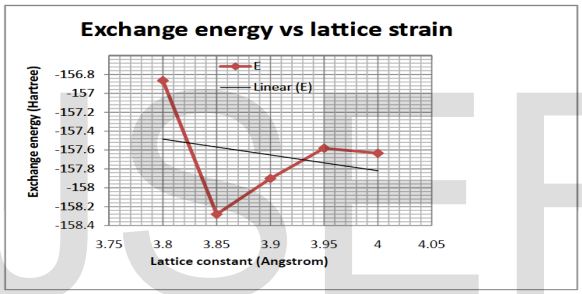

Figure 6: Exchange energy vs. lattice strain for cubic $BaMnO_3$. A decrease in exchange energy can be seen for the compression of lattice. There is smaller deviation from the linear trend.

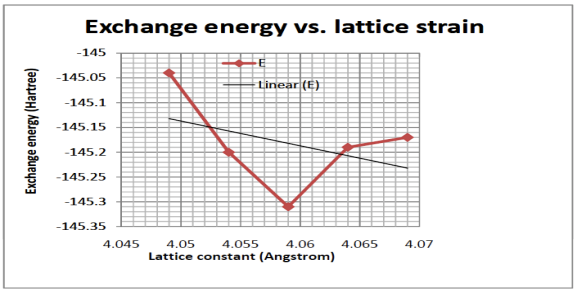

Figure 7: Exchange energy vs. lattice strain for cubic $BaVO_3$. A slight increase in the exchange energy can be seen for the compression of lattice. The nonlinear dependence of the exchange energy on lattice strain is more pronounced.

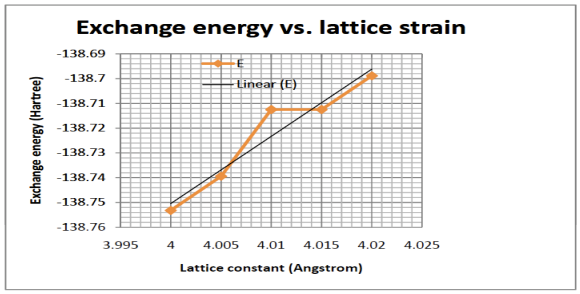

Figure 8: Exchange energy vs. lattice strain for cubic $BaTiO_3$. A decrease in exchange energy can be seen for the compression of lattice. The oscillatory character of exchange energy is also persistent.

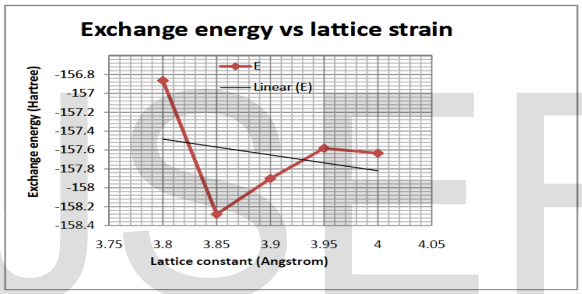

Figure 9: Exchange energy vs. lattice strain for cubic $BaMnO_3$. The nonlinear dependence of the exchange energy on the compression of lattice can be observed. Exchange energy has slightly increased with the compression of the lattice in this case.

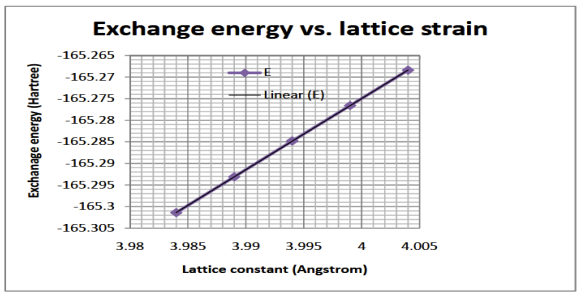

Figure 10: Exchange energy vs. lattice strain for cubic $BaFeO_3$. A decrease in exchange energy can be seen for the compression of lattice showing a linear dependence on the strain.

[2] Ce-Wen Nan-, M. I. Bichurin, Shuxiang Dong, D Viehland and G Sirinivasan, *Multiferroic magneto electric composites: Historical perspective, status, and future directions.*

[3]

[4] R. Dovesi, V. R. Saunders, C. Roetti, R. Orlando, C. M. Zicovich-Wilson, F. Pascale, B. Civalleri, K. Doll, N. M. Harrison, I. J. Bush, P. D'Arco, M. Llunell, University of Torino, Torino, Italy 2009.

[5] W. F. Perger, J. Criswell, B. Civalleri, R. Dovesi, Comput. Phy. Comm. 180 (2009) 1753.

[6] W. F. Perger, Int. J. Quantum Chem. 110 (2009) 1916.

[7] W. Marquardt, SIAM J. Appl. Math. 11 (1963) 431.

[8] F. D. Murnaghan, Proc. Natl. Acad. Sci. (USA) 30 (1944) 244.

[9] C. Gatti, V. R. Saunders, C. Roetti, J. Chem. Phys. 101 (1994) 10686.

[10] F. Corà, Mol. Phys.103 (2005) 2483.

[11] T. Bredow, K. Jug, R. A. Evarestov, Phys. Stat. Sol. 243 (2006) R10.

[12] , Noel W. Thomas,Acta. Cryst.,45,337-44,1989.

[13] , A. Bouhemadou and K. Haddadi, Solid State Sciences,12,630-36,2010

[14] , Nina Orlovskaya and Kjersti Kleveland and Tor Grande and Mari - Ann Einarsrud, Jrnl. European Cera. Soc., 20, 50-56, 1991.

[15] , Furio Corà, Molecular Physics, 103, 2483-2496, 2005.

[16] , Thomas Bredow and Karl Jug and Robert A. Evarestov, Phys. Stat. Sol., 243, R10-R12, 2006.

[17] , Abhay Shukla and E. D. Isaacs and D. R. Hamann and P. M. Platzman, Phy. Rev. B, 64, (052101)-1-4, 2001.

[18] Crystal06 software www.crystal.unito.it/.

[19] classical model, *Coupled Harmonic oscillator model.*

[20] A Sirinivas, R. Gopalan, V. Chandrasekhran, *Room Temperature multiferroism and magnetoelectric coupling in BaTiO3-BaFe12O19 system*

[21] A Sirinivas, R. Gopalan, V. Chandrasekhran, *Room Temperature multiferroism and magnetoelectric coupling in BaTiO3-BaFe12O19 system*

[22] Evgeny T Tsymbal et al, *Tailoring magnetic anisotropy at the ferromagnetic and ferroelectric interface*

[23] Evgeny T Tsymbal et al, *Interface e?ects in spin-polarized metal/insulator layered structures*

[24] Evgeny Y Tsymbal, Oleg N Mryasov and Patrick R LeClair, *Spin-dependent tunnelling in magnetic tunnel junctions*

[25] J. J. Sakurai, *Introduction to quantum physics*

[26] Charles Kittel, *Quantum Field Theory*

[27] Norobert Majlis, *The Quantum Theory of Magnetism*

[28] Qing Hua Qin, *Green's Function and Boundary Elements of Multifield Materials*

[29] Nicola A. Hill, *First principles study of Multi ferroic magneto electric Manganites*

[30] Kenichiro Ban, Manabu Gomi,Takeshi Shundo, D. I. Khomiskii, Multiferroics: *different ways to combine magnetism and ferroelectricity*

[31] Hans Schmid, On ferrotoroidics , Electrotoroidic, Magnetotoroidic and piezotoroidic effects

[32] Igor Zutic, Jarsalow Fabain, S Das sarma, Spintronics : *fundamentals and applications*

[33] Das: *Spin FET*

[34] Sankar Das Sarma, *Spintronics*

[35] Spintronics- *A retrospective and perspective*

[36] Daniel C Mattis, *The theory of magnetism*

[37] Chun-Gand Duan, Sitram S Jaswal, Evegeny Y Tsybmal, *towards ferroelectrically controlled magnetism: Magnetoelectric effect in Fe/BaTio3 multilayers*

[38] Manuel Bibes and Agnes Barthelemy, *Oxide spintronics*

[39] Piskinov et al , *Bulk properties and electronic structure of SrTiO3, BaTiO3, PbTiO3 perovskites: an ab initio study*

[40] V. K. Wadhawan, *Ferroic materials: A primer*

[41] Sinha and Upadhaya *Phonon-Magnon interaction in magnetic crystals*

[42] A.S. Verma and V.K. Jindal, *Lattice constant of cubic perovskites.*

[43] S. Piskunov, E. Heifets, R.I. Eglitis, G. Borstel, *Bulk properties and electronic structure of SrTiO3, BaTiO3, PbTiO3 perovskites: an ab initio HF/DFT study.*

[44] Takahisa Omata, Tomonao Fuke and Shinya Otsuka-Yao-Matsuoa, *Hydration behavior of Ba2Sc2O5 with an oxygen-deficient perovskite structure.*

[45] Shu-yao Yan and Ying Xie and Tao Liu and Hai-tao Yu, *Electronic structures and ferroelectric instabilities of cubic AVO3 (A = Sr, Ba, and Pb) perovskites by first-principles calculations.*

[46] Z. H. Zhu and X. H. Yana, *Half-metallic properties of perovskite* $BaCrO_3$ *and* $BaCr_{0.5}Ti_{0.5}O_3$ *superlattice: LSDA + U calculations*

[47] James M. Rondinelli and Aaron S. Eidelson and Nicola A. Spaldin, *Non-*d^0 *Mn-driven ferroelectricity in antiferromagnetic BaMnO3.*

[48] A. S. Verma ans A. Kumar, and S. R. Bhardwaj, *Correlation between ionic charge and the lattice constant of cubic perovskite solids.*

[49] Sumio Ishihara and Satoshi Okamoto and Sadamichi Maekawa, *Pressure effects in manganites with layered perovskite structure.*

[50] Yoshinori Tokura, *Correlated-electron physics in transition-metal oxides.*

[51] ,Yoshinori Tokura *etal Orbital physics in transition metal oxides.*

[52] J. B. Goodenough, *Electron-lattice interactions in Manganese oxide perovskites.*

[53] Charles Day, *Nanoscale phase competition accompanies Colossal magnetoresistance.*

[54] S. Maekawa, T. Tohyama, S.E. Barnes, S. Ishihara, W. Koshibae, G. Khaliulin, *Physics of Transition metal oxides, Chapter1, 4, 5 and 7.*

[55] C. N. Rao, B. Raveau, *Transition Metal Oxides, Structure, Properties, and Synthesis of Ceramic Oxides*

[56] Henrich and Cox, *The Surface Science of Metal Oxides.*

[57] Wolfram and Ellialtioglu, *Electronic and Optical Properties of d-Band Perovskites*

[58] Barbel Fromme, *d-d Excitations in Transition-Metal Oxides.*

[59] K. H. Ahn, T. Lookman,A. R. Bishop, *Strain-induced metal-insulator phase coexistence in perovskite manganites.*

[60] R. V. K. Mangalam, Nirat Ray, Umesh V. Waghmare, A. Sundaresan and C. N. R. Rao, *Multiferroic Properties of Nanocrystalline BaTiO3.*

[61] CRYSTAL09 Code,*www.crystal.unito.it.*

[62] Evgeny Y. Tsymbal et al, Tailoring magnetic anisotropy at the ferromagnetic and ferroelectric interface.

[63] Evgeny Y. Tsymbal et al, Interface effects in spin-polarized metal/insulator layered structures.

[64] Evgeny Y. Tsymbal, Oleg N Mryasov and Patrick R LeClair, *Spin-dependent tunnelling in magnetic tunnel junctions.*

[65] Chun-Gand Duan, Sitram S Jaswal, Evegeny Y. Tsybmal, *towards ferroelectrically - controlled magnetism: Magnetoelectric effect in Fe/BaTio3 multilayers.*

[66] A Sirinivas, R. Gopalan, V. Chandrasekhran, *Room Temperature multiferroism and magnetoelectric coupling in* $BaTiO_3 - BaFe_{12}O_{19}$ *system.*

[67] Manuel Bibes and Agnes Barthelemy, Oxide spintronics

[68] Norobert Majlis, *The Quantum Theory of Magnetism*

[69] Nicola A. Hill, *First principles study of Multi ferroic magneto electric Manganites.*

[70] Ramamurthy Shankar, *Fundamentals of quantum physics.*

[71] Charles Kittel, Quantum Field Theory

[72] P W Andesrson, H. Hasegawa, Considerations on Double Exchange.

[73] Z. G. Liu et al, *Room-temperature ferromagnetism and ferroelectricity in Fe-doped $BaTiO_3$*

[74] Xin Wiang and Qiliang Qui and Yuewu Pan and Guangtian Zou, *A possible phase separation scenario observed in perovskite Managanites under high pressure*

[75] Masahito Mochizuki,*Spin and orbital states and their phase transitions of the perovskite -type Ti xides: Weak coupling approach*

[76] J. J. Zuckerman, *Crystal Field Splitting Diagrams*

[77] Zhong,*Uniaxial Compressive Property of the Lattice of Colossal Magnetoresistance Perovskite Compound $La_xSr_{1-x}MnO_3$.*

[79] S. J. Youn, B. I. Min,*Half metallic electronic structures of colossal magnetoresistance Manganese Oxides.*

[79] S. J. Youn, B. I. Min, *Half metallic electronic structures of colossal magnetoresistance Manganese Oxides.*

[80] classical model, *Coupled Harmonic oscillator model.*

[81] A Sirinivas, R. Gopalan, V. Chandrasekhran, *Room Temperature multiferroism and magnetoelectric coupling in BaTiO3-BaFe12O19 system*

[82] A Sirinivas, R. Gopalan, V. Chandrasekhran, *Room Temperature multiferroism and magnetoelectric coupling in BaTiO3-BaFe12O19 system*

[83] Evgeny T Tsymbal et al, *Tailoring magnetic anisotropy at the ferromagnetic and ferroelectric interface*

[84] Evgeny T Tsymbal et al, *Interface e?ects in spin-polarized metal/insulator layered structures*

[85] Evgeny Y Tsymbal, Oleg N Mryasov and Patrick R LeClair, *Spin-dependent tunnelling in magnetic tunnel junctions*

[86] J. J. Sakurai, *Introduction to quantum physics*

[87] Charles Kittel, *Quantum Field Theory*

[88] Norobert Majlis, *The Quantum Theory of Magnetism*

[89] Qing Hua Qin, *Green's Function and Boundary Elements of Multifield Materials*

[90] Nicola A. Hill, *First principles study of Multi ferroic magneto electric Manganites*

[91] Ce-Wen Nan-, M. I. Bichurin, Shuxiang Dong, D Viehland and G Sirinivasan, *Multiferroic magneto electric composites: Historical perspective, status, and future directions*

[92] Kenichiro Ban, Manabu Gomi,Takeshi Shundo, D. I. Khomiskii, Multiferroics: *different ways to combine magnetism and ferroelectricity*

[93] Hans Schmid, On ferrotoroidics , Electrotoroidic, Magnetotoroidic and piezotoroidic effects

[94] Igor Zutic, Jarsalow Fabain, S Das sarma, Spintronics : *fundamentals and applications*

[95] Das: *Spin FET*

[96] Sankar Das Sarma, *Spintronics*

[97] Spintronics- *A retrospective and perspective*

[98] Daniel C Mattis, *The theory of magnetism*

[99] Chun-Gand Duan, Sitram S Jaswal, Evegeny Y Tsybmal, *towards ferroelectrically controlled magnetism: Magnetoelectric effect in Fe/BaTio3 multilayers*

[100] Manuel Bibes and Agnes Barthelemy, *Oxide spintronics*

[101] Piskinov et al , *Bulk properties and electronic structure of SrTiO3, BaTiO3, PbTiO3 perovskites: an ab initio study*

[102] V. K. Wadhawan, *Ferroic materials: A primer*

[103] Sinha and Upadhaya *Phonon-Magnon interaction in magnetic crystals*